

Contrastive Semi-Supervised Learning for 2D Medical Image Segmentation

Prashant Pandey¹, Ajey Pai¹, Nisarg Bhatt¹, Prasenjit Das², Govind Makharia², Prathosh AP¹, and Mausam¹

¹ Indian Institute of Technology, New Delhi, India.
 getprashant57@gmail.com, ajey.pai.karkala@ee.iitd.ac.in,
 nisarg.bhatt.cs117@cse.iitd.ac.in, prathoshap@ee.iitd.ac.in,
 mausam@cse.iitd.ac.in

² All India Institute of Medical Sciences, New Delhi, India.
 prasenaiims@gmail.com, govindmakharia@gmail.com

Abstract. Contrastive Learning (CL) is a recent representation learning approach, which achieves promising results by encouraging inter-class separability and intra-class compactness in learned image representations. Because medical images often contain multiple classes of interest per image, a standard image-level CL for these images is not applicable. In this work, we present a novel semi-supervised 2D medical segmentation solution that applies CL on image patches, instead of full images. These patches are meaningfully constructed using the semantic information of different classes obtained via pseudo labeling. We also propose a novel consistency regularization scheme, which works in synergy with contrastive learning. It addresses the problem of confirmation bias often observed in semi-supervised settings, and encourages better clustering in the feature space. We evaluate our method on four public medical segmentation datasets along with a novel histopathology dataset that we introduce. Our method obtains consistent improvements over the state-of-the-art semi-supervised segmentation approaches for all datasets.

Keywords: Semi-supervision, Contrastive Learning, Segmentation

1 Introduction

A key challenge in the use of modern deep learning systems for medical image segmentation is their need for large and annotation-rich training datasets. While semi-supervised methods address this problem by leveraging large unlabelled data [12,9,8,2], they are not designed to learn strong representations. Recently, contrastive learning (CL) has paved the path to learn strong representations from unlabelled data. Here, representations are learned such that an image and its transformations are similar while those of other images are dissimilar [1,6]. Our goal is to study the application of CL for semi-supervised segmentation. However, a key problem with CL methods is that the transformations are applied image-wise, which learns representations for images that have a single label; little is

known as to what representations are learnt for the case of *multi-label* semantic segmentation. Further, all contrastive methods work exclusively on immensely large datasets like ImageNet, which may not transfer well to medical domains due to domain shift and reduced number of data instances [14]. In this work, we address some of these issues while applying CL for medical image segmentation via the following contributions,

1. We propose a CL framework that uses pseudo labels on patch-wise embeddings corresponding to distinct semantic classes – this encourages inter-class separability and intra-class compactness of learned representations.
2. We propose a novel consistency regularization [16] scheme in tandem with CL: it addresses the problem of confirmation bias [3] often observed in semi-supervised methods. Further it also encourages better clustering in the feature space aiding CL.
3. We introduce a novel histopathology dataset of the human duodenum on which our method has been evaluated along with 4 publicly available datasets. In all datasets, our method significantly and consistently outperforms existing fully supervised as well as state-of-the-art semi-supervised approaches.

2 Prior work

Recent semi-supervised segmentation methods [12,2,21,8] use conventional loss functions like cross-entropy, mean squared error (MSE) or a number of their combinations as training objectives. It is reported that these loss functions do not help in learning strong representations [29]. In this work, we have shown that representation learning can help to improve the performance of semi-supervised segmentation through the use of contrastive learning (CL). CL is an unsupervised technique where an image representation is trained to be closer to its transformations, and farther from other random images in the dataset. An extension [7] contrasts examples of one class against those of other classes. Recently, CL has achieved state-of-the-art results on several tasks [1,6]. However, very little work is done on using CL for semantic image segmentation. To the best of our knowledge, only one work has utilized CL for segmentation of volumetric (3D) data [22], by contrasting between images at the same spatial location. This method cannot be applied to 2D image segmentation where temporal information is not available. Consistency regularization (CR) is another method in semi-supervised learning which assumes that decision boundaries lie in the low density regions of the data-distribution [27]. A recent work [16] tries to move the decision boundaries to low-density regions of the data distribution using CR. We show that CR aids CL in doing better feature clustering which helps in effective delineation of decision boundaries in the feature space.

3 Proposed methodology

Consider a dataset \mathcal{D} with $\mathcal{D}_L = \{(x_1, y_1), (x_2, y_2), \dots, (x_t, y_t)\}$ as the small pixel-wise labelled set of images (where (x_i, y_i) is an image-mask pair) with every

pixel in x_i belonging to one of C semantic classes and a large unlabelled set $\mathcal{D}_U = \{x_1^u, x_2^u, x_3^u, \dots, x_m^u\}$ where $t \ll m$. Initially, a fully supervised network with U-Net like architecture [17] (with encoder E_θ and decoder D_θ parameterized by θ) is trained (please refer Fig.1) for semantic segmentation on \mathcal{D}_L using the following loss function: $\mathcal{L}_{sup} = H(D_\theta(E_\theta(x_i)), y_i)$, where H is the standard cross-entropy loss.

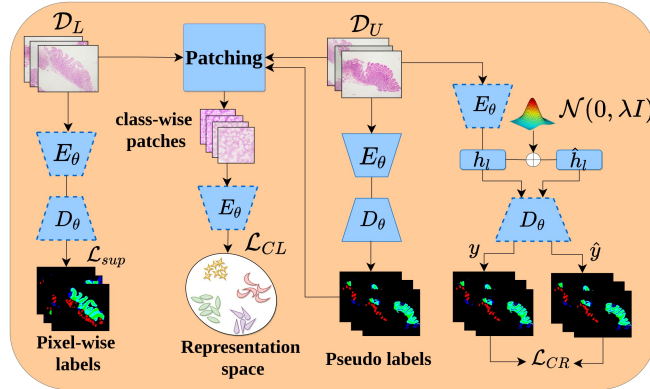


Fig. 1. The proposed Contrastive Semi-Supervised Learning method. **A)** For labeled data \mathcal{D}_L , fully-supervised encoder E_θ and decoder D_θ are trained with \mathcal{L}_{sup} . **B)** Trained E_θ and D_θ generate pseudo labels on unlabelled data \mathcal{D}_U . **C)** These are used to sample class-wise patches from \mathcal{D}_U to retrain E_θ for contrastive learning with \mathcal{L}_{CL} . **D)** Paralelly, consistency regularization is employed on \mathcal{D}_U to learn similar outputs on various perturbations \hat{h}_l of image features h_l using \mathcal{L}_{CR} . The same encoder-decoder pair are trained at every stage. Dotted outlines indicate that the respective component is being trained in that step.

Patching: Here we explain our strategy to extract class-wise patches using pseudo labels. The supervised network is used to generate pseudo labels on \mathcal{D}_U . Using class-wise pseudo labels of \mathcal{D}_U along with ground-truth masks of \mathcal{D}_L , we sample class-wise patches of fixed size from the images for contrastive learning [7]. Let $g_\theta : W \rightarrow C$ and $\tilde{g}_\theta : Z \rightarrow C$ be two functions which are being learnt that assign classes in C to a patch in W and an embedding in Z , respectively using the neural network. For every patch w_i ($w_i \in W$, $g_\theta(w_i) \in C$), class-wise unit normalised patch embedding $z_i = E_\theta(w_i)$ ($\tilde{g}_\theta(z_i) = g_\theta(w_i)$, $z_i \in Z$) is obtained.

Contrastive learning: Next, we explain how we perform contrastive learning in our method on class-wise image patches. A supervised contrastive loss is computed for all the patch embeddings as,

$$\mathcal{L}_{CL} = \frac{-1}{|W|} \sum_{i=1}^{|W|} \frac{1}{P} \sum_{z_p \in Z_p} \log \frac{\exp(z_i^T \cdot z_p)}{\exp(z_i^T \cdot z_p) + \sum_{k=1}^{|Q^{(i)}|} \exp(z_i^T \cdot z_k)} \quad (1)$$

Where $|W|$ is the total number of patches sampled in a batch of images. $P \subseteq C$ is the number of classes in a batch of patches. $Z_p = \{z_p : \tilde{g}_\theta(z_p) = \tilde{g}_\theta(z_i)\} \setminus z_i$. Each $z_k \in Q^{(i)}$ where $Q^{(i)}$ is the set of *all* negative examples for z_i . We define $Q^{(i)} = \{Q_N^{(i)} \cup Q_H^{(i)}\}$ where $Q_N^{(i)}$ is the total number of negative examples ($\{z_n\}$) belonging to class $\tilde{g}_\theta(z_n)$ such that $\tilde{g}_\theta(z_n) \neq \tilde{g}_\theta(z_i)$. Whereas $Q_H^{(i)}$ is the set of all hard negatives ($\{z_n^h\}$) generated by taking motivation from [15]. For datasets having at least two semantic classes, we perform the hard negative mining by interpolating a patch embedding z_i with all other negative patch embeddings $\{z_n\}$ in the following way: $z_n^h = \alpha z_i + (1 - \alpha)z_n$ where $\alpha \sim (0, 0.4)$ is chosen to ensure that the contribution of z_i is lesser than the negative example z_n . When there is only a single semantic class in the dataset \mathcal{D} , a unit normalised Gaussian distribution $\mathcal{N}(\mu, \Sigma)$ with fixed μ and Σ and the same dimensionality as that of z_i is randomly defined. It acts as the auxiliary negative class for the real class in the dataset \mathcal{D} . All the required negative examples $\{z_n\}$ are sampled from this distribution and interpolated with z_i . The \mathcal{L}_{CL} loss encourages inter-class separation and intra-class compactness of the unit-normalised patch embeddings in the representation space.

Consistency regularization: Here, we formulate our consistency regularization scheme that aids in better contrastive learning. Semi-supervised learning methods that rely on pseudo labels suffer from confirmation bias [3]. As shown by [11], choosing pseudo labels with high confidence threshold and strong data augmentation alleviates this problem and improves the quality of pseudo labels on the unlabelled data. Following this strategy for sampling class-wise patches, we have kept a high pixel activation threshold. However, [4] argues that in the semantic segmentation setting, the cluster assumption is violated since the decision boundaries at the low density regions do not align with class boundaries in the input space. It also states that the semantic class decision boundaries are more discernible in the feature space making feature level perturbations more suitable for semantic segmentation. To this end, we propose a consistency regularization strategy that delineates decision boundaries in the feature space by aiding CL. Initially, as the pseudo labels are noisy, the image embeddings are perturbed mildly and as the class-wise clusters improve with contrastive learning in the representation space, the severity of perturbation is increased. To achieve this, image embeddings $h_l = E_\theta(x_i^u)$ are obtained by passing image $x_i^u \in \mathcal{D}_U$ through the encoder E_θ . We perturb h_l to obtain \hat{h}_l where $\hat{h}_l = h_l + r$. The perturbation r is sampled from a unit normalised Gaussian with a scaled variance as: $r \sim \mathcal{N}(0, \lambda I)$. The scaling λ is called the adjusted Silhouette coefficient[10]. It depends on the quality of the feature clusters in the representation space given by: $\lambda = \frac{\omega+1}{2} + \epsilon$. Here, ϵ is a small non-negative value and $\omega \in [-1, 1]$ is the Silhouette coefficient. It is a metric used to measure the goodness of clustering and is given by: $\omega = \frac{d(b,a)}{\max(b,a)}$, where b is the average distance between any two clusters in the feature space, a is the variance in the reference cluster and $d(\cdot)$ is the Manhattan distance.

With improving cluster quality, the severity of the perturbations on h_l increases thereby generating harder perturbations. After measuring the goodness

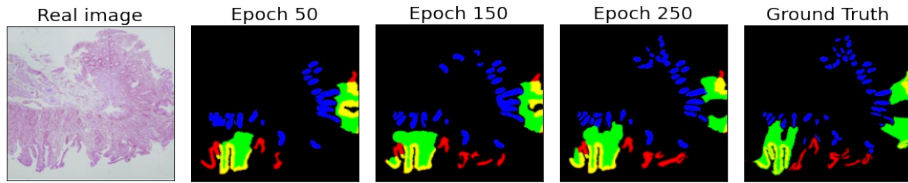


Fig. 2. Pseudo label refinement during model training on duodenal dataset.

of the clustering in the representation space we decode h_l to obtain y_l from the previous version of the network parameters while \hat{h}_l is decoded with the concurrent version of the network parameters to obtain \hat{y}_l . Then, we force the decoder to make \hat{y}_l consistent with y_l with varying degrees of feature perturbations using the following loss function to achieve robust consistency regularization: $\mathcal{L}_{CR} = \frac{1}{B} \sum_{l=1}^B H(y_l, \hat{y}_l)$ where B is the batch size. The total loss then becomes: $\mathcal{L}_{tot} = \mathcal{L}_{CL} + \mathcal{L}_{CR}$. The neural network is fine-tuned on \mathcal{D}_L at interleaving epochs and update the weights for semantic segmentation. In this way, the contrastive learning and the consistency regularization steps are repeated until \mathcal{L}_{tot} converges. By training the network in this manner, we ensure that distinct semantics are clustered compactly while ensuring better performance on unlabelled data. Fig.2 shows pseudo label refinement through different epochs for an example from our duodenal histopathology dataset.

4 Implementation details and hyperparameter choice

Attention U-Net [28] is taken as the backbone for segmentation. Its encoder-decoder architecture is scaled across the channels to match the size and complexity of vanilla U-Net [17], which is widely used as a comparison baseline. This ensures that the model complexity is not unfairly advantageous to us. For fine-tuning, a batch size of 16 images having dimensions 320×256 is used with Adam optimiser. The initial learning rate is $1e-3$ with a learning rate scheduling of $0.1 \times$ reduction at every loss plateau. For contrastive learning, a batch size of 816 patches (largest size possible) and for consistency regularization, 8 full images are used from which patches are sampled. The negative keys are interpolated with their queries to generate hard negative samples on the fly. The generated negative samples are used as additional negatives in the batch. This technique and a fairly large batch size helps us avoid a memory bank or queue for storing negative samples. We use an octa-core system with 16GB RAM and 32GB V100 Nvidia GPU. Our code is implemented in Keras with TensorFlow (2.0+) backend.

Hyperparameters for our model are selected based on model performance on validation data. Only those patches are chosen which have a minimum number of pixel activations above a threshold set at the first training iteration. For all experiments, we chose a minimum of 25 pixels as the qualification criteria for a patch. All the codes, some sample images of our novel dataset are available [here](#).

Hyperparameter sensitivity analysis: The confidence threshold of pixel activations while pseudo labels are generated is a hyperparameter. As stated in [11], high confidence thresholds are needed so that the problem of confirmation bias is mitigated. To choose a threshold, a Precision-Recall curve was plotted for the first training iteration and a threshold value which yielded maximum dice score on validation data was fixed throughout the rest of training process. The second hyperparameter in our model is ϵ . This was chosen such that it isn't too large when compared to $\frac{\omega+1}{2}$ nor too small. A small value will lead to very weak perturbations for consistency regularization during the initial training epochs. On the other hand, if a large value is chosen, $\frac{\omega+1}{2}$ will become negligible and nearly a constant perturbation is applied to the features.

Table 1. Performance evaluation (Avg. Dice Score on 3 runs) on duodenal histopathology dataset compared with a prior art [21] and full supervision [28].

Duodenal Histopathology			
Tissue	Fully Supervised	TCSM.v2 [21]	Ours
Crypts	39.5±0.8	51.1±0.8	61.5±0.5
Villi	47.8±0.6	53.4±0.4	61.2±0.1
Epithelium	50.6±0.3	60.9±0.2	68.6±0.5
Brunner's Gland	79.7±0.5	86.2±0.8	88.6±0.2
Average	54.4±0.6	62.4±0.6	69.9±0.3

5 Experiments

We use five medical segmentation datasets in our experiments.

Duodenal Histopathology Dataset - We introduce a novel histopathological dataset of the human duodenum. Duodenum is the upper tract of the small intestines. It contains 1150 unlabelled and 110 labelled H&E stained histological images of resolution 2448×1920 pixels each with four tissue classes - Villi, Crypts, Epithelium and Brunner's Gland annotated and verified by expert gastroenterologists. The images are captured through an Olympus BX50 microscope at $4 \times$ zoom using a DP26 camera. Ethical clearance was obtained which will be provided post acceptance (to maintain anonymity). We use 50 labeled images and randomly make a 70-30 split to get a training and validation set. The rest of the labeled set is utilized as unlabeled examples along with 1150 unlabeled images. A separate set of 60 labeled images are used for testing. A four-class semantic-segmentation (Table 1) task is performed and our method is compared with [21] and a fully-supervised model [28]. We trained [21] on our histopathology dataset and evaluated its test time performance. This method is a recent state-of-the-art on multiple 2D image datasets. We reimplemented the method using Attention-Unet as the backbone for fair comparison. After grid search, we find the smoothing co-efficient α to be 0.9.

Table 2. Average Dice scores on MoNuSeg and CHAOS dataset (validation) for different amounts of labelled data used. For MoNuSeg, our primary baseline is [2]. For CHAOS, DAFNet [18] is our primary baseline method that utilizes unlabelled samples from T2 as well as T1 scans from the dataset. We use only T2.

MoNuSeg				CHAOS			
Method	20%	50%	100%	Method	50%	25%	13%
Fully Supervised	71.9	77.7	79.3	Unet [17]	80.1	76.1	72.1
SoftMax [12]	73.65	76.1	–	SDNet [19]	82.1	77.1	75.1
MC Dropout [8]	75.3	77.9	–	Fully-Supervised	83.5	81.4	77.9
Self-Loop [2]	77.1	79.1	–	DAFNet [18]	84.0	82.0	79.0
Ours	79.5 ± 0.4	80.4 ± 0.2	–	Ours	86.9 ± 0.2	85.9 ± 0.4	82.3 ± 0.6

CHAOS Dataset [26] - The dataset consists of 623 T2 SPIR MRI scans. We perform T2 segmentation task of four classes: Liver, left kidney, right kidney and spleen. The labelled data is first split into 70-30 train-val split randomly. A variable number of samples from train split are taken as labelled samples and rest as unlabelled samples for semi-supervised learning in our method (Table 2)

MoNuSeg Dataset [23] - Consists of 30 H&E stained training images and 14 test images of tissues from several organs. We perform nuclei segmentation by using different amounts of labelled samples from the train set, with an 80-20 train-val split and utilize the rest of them as unlabelled samples for semi-supervised learning and compare it with the methods in [23] (Table 2).

JSRT Dataset [13] - Consists of 247 posterior-anterior chest radiographs. We perform semantic segmentation of three classes - Lungs, heart and clavicles. We split the data into labelled and unlabelled sets of variable size. The labelled set itself is split into 80-20 train-val sets for supervised training steps and unlabelled images are used for semi-supervision. 5-fold mean accuracy and standard deviation is reported over the train-val splits. The results are shown in Table 3.

IDRiD Dataset [20] - provides pixel level multi-lesion annotations of Diabetic Retinopathy (DR). It has 81 color fundus images with DR symptoms that are split into 54 training and 27 testing images. In Table 4, we compare our method on this dataset with [24]. Our experiments are designed according to its setup except that we do not train a classification model.

Experiments on different datasets show the effectiveness of our method. For each dataset, comparisons are done with the latest and SOTA semi-supervised methods. For MoNuSeg dataset, we outperform a very recent state-of-the-art method (Self loop uncertainty) by 2.5% dice score on few labelled images. On CHAOS dataset, we outperform DAFNet by 3.0% dice score which also uses images from other modalities to improve performance. On JSRT dataset, our method outperforms SemiTC and gains 4.0% increment on IoU scores. For IDRiD dataset, we gain improvement on AUC_PR score for every class.

5.1 Ablation Studies

We perform detailed ablation on the MoNuSeg dataset with 50% of the labeled images. It was observed that when consistency regularisation is employed with-

Table 3. Comparison of our method with baseline [9] on JSRT dataset for semantic segmentation. The reported metric is mean IoU with standard deviation for 3 runs. We perform student’s unpaired t-test to show statistical significance of our results.

JSRT				
Method	Amount of \mathcal{D}_L	Amount of \mathcal{D}_U	mIoU	p-value
Human	–	–	90.66 ± 3.6	–
MSNet [5]	24	100	67	–
MSNet	124	0	81	–
SemiTC [9]	25	99	88.7 ± 1.0	–
SemiTC	50	74	89.7 ± 0.2	–
Fully-Supervised	25	99	86.5 ± 1.3	–
Fully-Supervised	50	74	88.1 ± 0.4	–
Ours	25	99	91.7 ± 0.5	0.0072
Ours	50	74	94.1 ± 0.3	0.0033

Table 4. Performance comparison of our method with baseline [24] for semantic segmentation. The reported metric is Area under the Precision-Recall curve (AUC_PR).

IDRiD				
Method	Microaneurysms	Haemorrhages	Hard Exudates	Soft Exudates
ASDNet [25]	0.4782	0.6285	0.8095	0.6924
CLSSSD[24]	0.4886	0.6812	0.8757	0.7337
Ours	0.4942	0.701	0.912	0.763

out the contrastive training step, the performance is close to the fully supervised model (Refer Table 1 in supplementary). We hypothesize that if consistency regularization is applied without contrastive learning, the pseudo labels that are generated as targets (y_l) are noisy with no scope for refinement in successive epochs. Moreover, the perturbations that are done to the feature embeddings h_l are wholly dependent on ϵ which is a constant. Therefore, the model isn’t able to learn consistent predictions on different perturbations and leverage unlabeled data. Whereas, it was found that without consistency regularization, the clustering quality ω doesn’t converge well (refer Fig.2 in supplementary). However, the performance is better than the fully-supervised model if contrastive learning is done with hard negative mining. This may be due to the fact that harder negatives help in delineating the class boundaries at low density regions when compared to simple negative examples. While hard negative mining also improves the performance when done with consistency regularization, performing all four together yields the most significant results.

6 Conclusion

This paper presents a semi-supervised representation learning scheme for semantic segmentation tasks in low data regime (especially medical imaging). We propose a novel method to utilize a large corpus of unlabelled images by using

contrastive training strategy, guided patching methods and consistency regularization of segmentation maps between learned and perturbed feature embeddings based on network’s clustering performance. We use hard negative mining to alleviate the bottlenecks associated with small batch sizes or absence of a memory bank during contrastive learning. Future iterations of this work will attempt to provide medical segmentation for 3D modalities.

References

1. Chen, T., Kornblith, S., Norouzi, M. and Hinton, G., 2020, November. A simple framework for contrastive learning of visual representations. In *International conference on machine learning* (pp. 1597-1607). PMLR.
2. Li, Y., Chen, J., Xie, X., Ma, K. and Zheng, Y., 2020, October. Self-Loop Uncertainty: A Novel Pseudo-Label for Semi-supervised Medical Image Segmentation. In *International Conference on Medical Image Computing and Computer-Assisted Intervention* (pp. 614-623). Springer, Cham.
3. Cascante-Bonilla, P., Tan, F., Qi, Y. and Ordonez, V., 2020. Curriculum Labeling: Revisiting Pseudo-Labeling for Semi-Supervised Learning. *arXiv preprint arXiv:2001.06001*.
4. Ouali, Y., Hudelot, C. and Tami, M., 2020. Semi-supervised semantic segmentation with cross-consistency training. In *Proceedings of the IEEE/CVF Conference on Computer Vision and Pattern Recognition* (pp. 12674-12684).
5. Shah, M.P., Merchant, S.N. and Awate, S.P., 2018, September. MS-Net: mixed-supervision fully-convolutional networks for full-resolution segmentation. In *International Conference on Medical Image Computing and Computer-Assisted Intervention* (pp. 379-387). Springer, Cham.
6. Cai, Q., Wang, Y., Pan, Y., Yao, T. and Mei, T., 2020. Joint contrastive learning with infinite possibilities. *arXiv preprint arXiv:2009.14776*.
7. Khosla, P., Teterwak, P., Wang, C., Sarna, A., Tian, Y., Isola, P., Maschinot, A., Liu, C. and Krishnan, D., 2020. Supervised contrastive learning. *arXiv preprint arXiv:2004.11362*.
8. Sedai, S., Antony, B., Rai, R., Jones, K., Ishikawa, H., Schuman, J., Gadi, W. and Garnavi, R., 2019, October. Uncertainty guided semi-supervised segmentation of retinal layers in OCT images. In *International Conference on Medical Image Computing and Computer-Assisted Intervention* (pp. 282-290). Springer, Cham.
9. Bortsova, G., Dubost, F., Hogeweg, L., Katramados, I. and de Bruijne, M., 2019, October. Semi-supervised medical image segmentation via learning consistency under transformations. In *International Conference on Medical Image Computing and Computer-Assisted Intervention* (pp. 810-818). Springer, Cham.
10. Kaufman, L. and Rousseeuw, P.J., 2009. *Finding groups in data: an introduction to cluster analysis* (Vol. 344). John Wiley & Sons.
11. Sohn, K., Berthelot, D., Li, C.L., Zhang, Z., Carlini, N., Cubuk, E.D., Kurakin, A., Zhang, H. and Raffel, C., 2020. Fixmatch: Simplifying semi-supervised learning with consistency and confidence. *arXiv preprint arXiv:2001.07685*.
12. Bai, W., Oktay, O., Sinclair, M., Suzuki, H., Rajchl, M., Tarroni, G., Glocker, B., King, A., Matthews, P.M. and Rueckert, D., 2017, September. Semi-supervised learning for network-based cardiac MR image segmentation. In *International Conference on Medical Image Computing and Computer-Assisted Intervention* (pp. 253-260). Springer, Cham.

13. J. Shiraishi, S. Katsuragawa, J. Ikezoe, T. Matsumoto, T. Kobayashi, K. Komatsu, M. Matsui, H. Fujita, Y. Kodera, and K. Doi, "Development of a digital image database for chest radiographs with and without a lung nodule: receiver operating characteristic analysis of radiologists' detection of pulmonary nodules", *American Journal of Roentgenology*, vol. 174, p. 71-74, 2000.
14. Zhou, Z., Sodha, V., Siddiquee, M.M.R., Feng, R., Tajbakhsh, N., Gotway, M.B. and Liang, J., 2019, October. Models genesis: Generic autodidactic models for 3d medical image analysis. In *International Conference on Medical Image Computing and Computer-Assisted Intervention* (pp. 384-393). Springer, Cham.
15. Kalantidis, Y., Sariyildiz, M.B., Pion, N., Weinzaepfel, P. and Larlus, D., 2020. Hard negative mixing for contrastive learning. *arXiv preprint arXiv:2010.01028*.
16. Verma, V., Lamb, A., Kannala, J., Bengio, Y. and Lopez-Paz, D., 2019. Interpolation consistency training for semi-supervised learning. *arXiv preprint arXiv:1903.03825*.
17. Ronneberger, O., Fischer, P. and Brox, T., 2015, October. U-net: Convolutional networks for biomedical image segmentation. In *International Conference on Medical image computing and computer-assisted intervention* (pp. 234-241). Springer, Cham.
18. Chartsias, A., Papanastasiou, G., Wang, C., Semple, S., Newby, D.E., Dharmakumar, R. and Tsaftaris, S.A., 2020. Disentangle, align and fuse for multimodal and semi-supervised image segmentation. *IEEE transactions on medical imaging*.
19. Chartsias A, Joyce T, Papanastasiou G, Semple S, Williams M, Newby DE, Dharmakumar R, Tsaftaris SA. Disentangled representation learning in cardiac image analysis. *Med Image Anal.* 2019 Dec;58:101535. doi: 10.1016/j.media.2019.101535. Epub 2019 Jul 18. PMID: 31351230; PMCID: PMC6815716.
20. Porwal, P., Pachade, S., Kamble, R., Kokare, M., Deshmukh, G., Sahasrabudhe, V. and Meriaudeau, F., 2018. Indian diabetic retinopathy image dataset (IDRiD): a database for diabetic retinopathy screening research. *Data*, 3(3), p.25.
21. Li, X., Yu, L., Chen, H., Fu, C.W., Xing, L. and Heng, P.A., 2020. Transformation-consistent self-ensembling model for semisupervised medical image segmentation. *IEEE Transactions on Neural Networks and Learning Systems*.
22. Chaitanya, K., Erdil, E., Karani, N. and Konukoglu, E., 2020. Contrastive learning of global and local features for medical image segmentation with limited annotations. *arXiv preprint arXiv:2006.10511*.
23. N. Kumar et al., "A Multi-Organ Nucleus Segmentation Challenge," in *IEEE Transactions on Medical Imaging*, vol. 39, no. 5, pp. 1380-1391, May 2020, doi: 10.1109/TMI.2019.2947628.
24. Zhou, Y., He, X., Huang, L., Liu, L., Zhu, F., Cui, S. and Shao, L., 2019. Collaborative learning of semi-supervised segmentation and classification for medical images. In *Proceedings of the IEEE/CVF Conference on Computer Vision and Pattern Recognition* (pp. 2079-2088).
25. Nie, D., Gao, Y., Wang, L. and Shen, D., 2018, September. ASDNet: attention based semi-supervised deep networks for medical image segmentation. In *International conference on medical image computing and computer-assisted intervention* (pp. 370-378). Springer, Cham.
26. A.E. Kavur, N.S. Gezer, M. Barış, S. Aslan, P.-H. Conze, et al. "CHAOS Challenge - combined (CT-MR) Healthy Abdominal Organ Segmentation", *Medical Image Analysis*, Volume 69, 2021. <https://doi.org/10.1016/j.media.2020.101950>
27. French, G., Laine, S., Aila, T., Mackiewicz, M. and Finlayson, G., 2020. Semi-supervised semantic segmentation needs strong, varied perturbations. In *British Machine Vision Conference* (No. 31).

28. Oktay, O., Schlemper, J., Folgoc, L.L., Lee, M., Heinrich, M., Misawa, K., Mori, K., McDonagh, S., Hammerla, N.Y., Kainz, B. and Glocker, B., 2018. Attention u-net: Learning where to look for the pancreas. arXiv preprint arXiv:1804.03999.
29. Gamaleldin F. Elsayed, Dilip Krishnan, Hossein Mobahi, Kevin Regan, and Samy Bengio. Large margin deep networks for classification. In Adv. Neural Inform. Process. Syst., 2018

A Additional Results

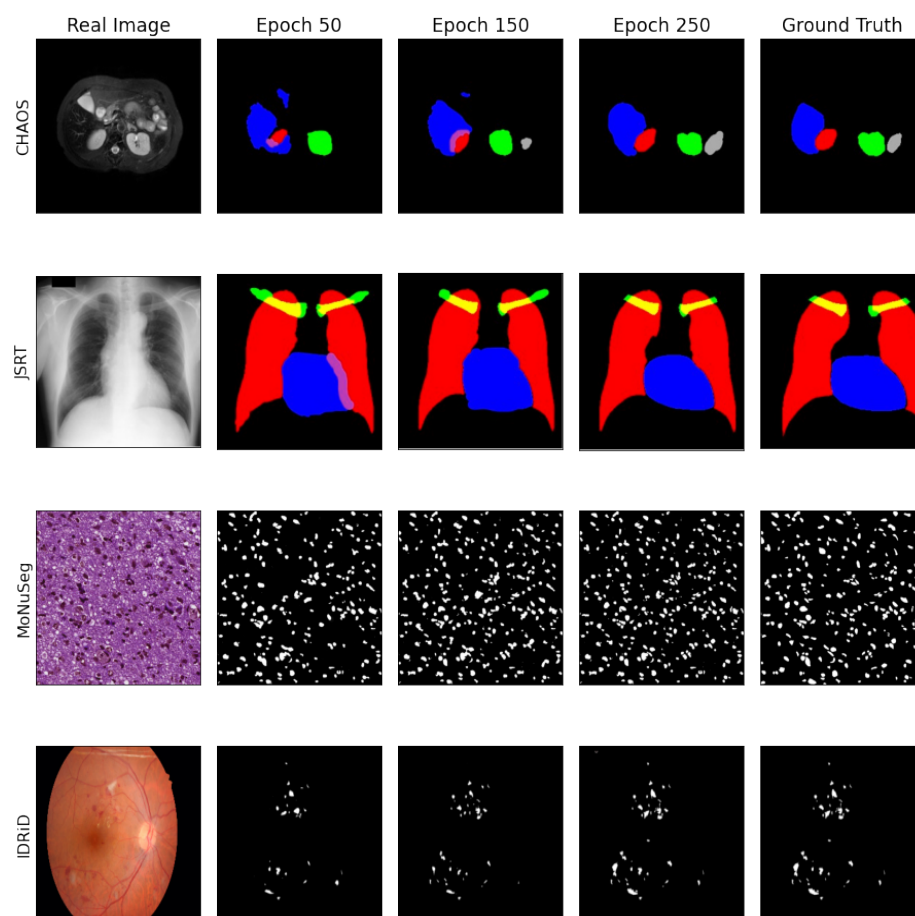
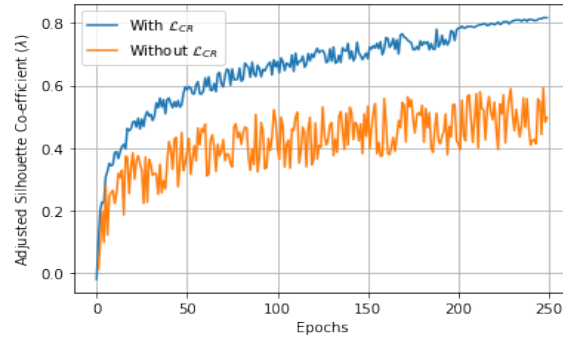
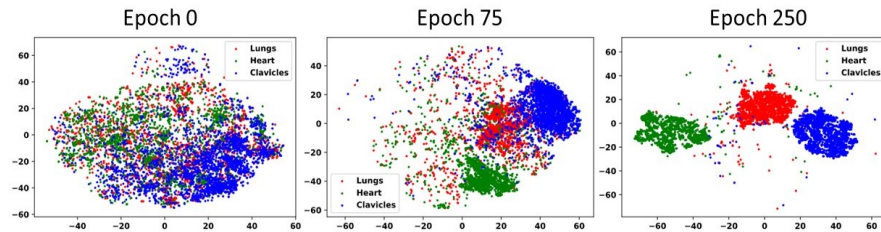


Fig. 3. Pseudo-label refinement during training for some publicly available datasets.

Table 5. Ablation on different components of our method during training and inference (HNM is Hard Negative Mining) for MoNuSeg dataset.

\mathcal{L}_{sup}	\mathcal{L}_{CL}	\mathcal{L}_{CR}	HNM	Dice
✓	✗	✗	✗	77.77
✓	✗	✓	✗	77.82
✓	✓	✗	✗	78.26
✓	✓	✗	✓	78.44
✓	✓	✓	✗	79.67
✓	✓	✓	✓	80.40

**Fig. 4.** Improvement of cluster quality during successive contrastive training epochs with \mathcal{L}_{CR} and without \mathcal{L}_{CR} for MoNuSeg dataset.**Fig. 5.** t-SNE plots of encoder patch embeddings for 3 classes from JSRT dataset during contrastive training at different training epochs. With the improvement of overall clustering, the silhouette coefficient increases.